PHYSICAL REVIEW E **92**, 040201(R) (2015)

Anisotropy of weakly vibrated granular flows

Geert H. Wortel and Martin van Hecke
Huygens-Kamerlingh Onnes Lab, Universiteit Leiden, Postbus 9504, 2300 RA Leiden, The Netherlands
(Received 16 October 2014; revised manuscript received 3 August 2015; published 28 October 2015)

We experimentally probe the anisotropy of weakly vibrated flowing granular media. Depending on the driving parameters—flow rate and vibration strength—this anisotropy varies significantly. We show how the anisotropy collapses when plotted as a function of the driving stresses, uncovering a direct link between stresses and anisotropy. Moreover, our data suggest that for small anisotropies, the shear stresses vanish. Anisotropy of the fabric of granular media thus plays a crucial role in determining the rheology of granular flows.

DOI: 10.1103/PhysRevE.92.040201 PACS number(s): 45.70.−n, 47.57.Gc, 83.80.Fg

The flow and spatiotemporal organization of granular media are intimately connected. Flow induces dilation [1–3], mechanical agitations [4–6], and anisotropy [2,7–12], which in turn strongly effect granular rheology [2,4–7,13–18]. Our understanding of this micro-macro coupling has made enormous steps, leading to predictive theories for the stationary flow of granular media [4–6,13–15,19]. What is missing is an understanding of nonstationary dense granular flows and a deeper understanding of the role of anisotropy.

For nonsteady flows, the anisotropy evolves during the duration of the experiment, and this leads to new phenomena that are not properly understood. In particular shear reversal experiments have shown that the buildup of anisotropy has a profound effect on the flow of granular media. After flow reversal, the shear stress drops to a low value, and the system compacts, after which the system dilates, and the shear stress increases back to its steady state value [2,7]. The qualitative picture that has emerged is that flow induces anisotropy which increases the resistance to flow, and then after reversal, the medium needs to be sheared over a finite strain before it reorganizes into a new state with opposite anisotropy.

How to access this anisotropy? In numerical simulations, anisotropies of the contact forces can readily be observed [20], even when the real-space fabric remains isotropic [21]. Experimentally, symmetry-breaking force chains can be visualized in two-dimensional flows using photoelastic particles [8,22]. It is very difficult to access these anisotropies in three-dimensional (3D) experiments. Moreover, we are not aware of experimental protocols that allow manipulating the level of anisotropy systematically. The precise role of anisotropy and how strongly it influences granular flows thus remain unclear.

Here we use a combination of rheology and vibrations to both *probe and control* the anisotropy of 3D granular flows. In essence, we use the rate of relaxation under weak probe vibrations as a proxy for the anisotropy. First, we show that supplying a steady granular flow with weak vibrations allows for tuning the anisotropy over a wide range [23,24]. This can be understood intuitively by the opposing effect of flow and vibrations on anisotropy: Flow is a symmetry-breaking field and tends to increase the anisotropy (until a steady state is reached), and vibrations tend to relax the system back to an isotropic state. Second, we introduce an experimental protocol which does not rely on real-space determination of the positions or forces between the grains to probe the anisotropy. Instead, we carefully stop the flow, "freezing" its fabric and then use vibrations to measure the relaxation of its anisotropy back to a more isotropic state. We find that the rate of relaxation under the same vibration conditions can vary over several decades: The stronger the anisotropy, the faster the relaxation.

Using this protocol, we show that in frozen samples under vibrations, the anisotropy decays as a universal logarithmic function of time. This allows us to accurately determine the relaxation rate at the start of the probe experiments, which we take as a proxy for the anisotropy. Second, we show that the anisotropy measured for a wide range of flow conditions can be collapsed when plotted as functions of the stress, revealing a deep link between anisotropy and resistance to flow. Finally, our data suggest that the resistance to stress vanishes when the anisotropy vanishes, consistent with the low stresses observed just after shear reversal. Anisotropy is thus a crucial aspect of granular flows.

Setup. We employ our recently developed granular vibrheology system [Fig. 1(a)], which allows rheological measurements on weakly vibrated granular media in a split-bottom geometry [23–25]. All our experiments are carried out in the same weakly vibrated split-bottom rheological cell as detailed in Ref. [24]—see Fig. 1(a). Briefly, in this setup the rotation of a rough disk of radius $r_s = 4$ cm at the bottom of a cylindrical cell drives a wide shear zone in the bulk of a layer (depth H) of black soda-lime glass beads of diameters between 1 and 1.3 mm. This disk is coupled to an Anton Paar DSR 301 rheometer, allowing us to perform experiments either at fixed torque T or at fixed rotation rate Ω. In the absence of vibrations, the flow profile is determined by the ratio H/r_s, which we fix at 0.33. In this regime, the shear bands are mainly vertical, and all grains above the disk corotate along with it (trumpet flow) [25]. The experimental cell is vertically vibrated at a fixed frequency of 63 Hz by a VTS system VG100 shaker where care is taken to decouple the rheometer from these vibrations [24]. The amount of vibrations is characterized by the dimensionless parameter $\Gamma = A(2\pi f)^2/g$, where A is the shaking amplitude, f is the frequency, and g is the gravitational acceleration—we focus on $0 < \Gamma < 1$.

Protocol. The experimental protocol to measure the anisotropy is outlined in Fig. 1(b) and consists of three main stages: *(S) Preparation of a sheared state:* Before each experiment we "refresh" the sample, by preshearing the system (not shown in Fig. 1) by three consecutive rapid (1 rps) shear motions in opposing directions, e.g., 5 s counter(co) clockwise, 10 s co(counter) clockwise, and 5 s counter(co) clockwise, after which there is a waiting period of 10 s during which

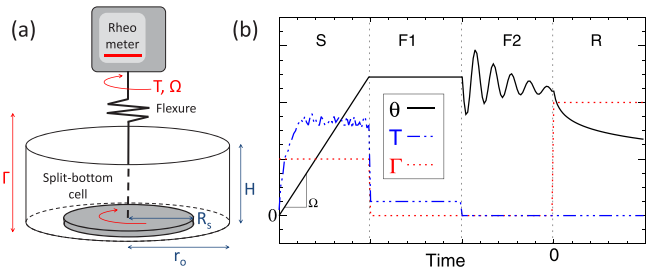

FIG. 1. (Color online) (a) Schematic of our vibrheological setup where a rheometer drives granular flow in a weakly vibrated container. Here T, Ω, and Γ are the driving torque, rotation rate, and dimensionless vibration strength, and R_s, r_0, and H are the radius of driving disk, radius of container, and filling height of the granulate. (b) A schematic of the measuring protocol, where θ is the angle of the driving disk. We distinguish four phases, labeled "S" for shear, "F1" for a "frozen" granulate with $\Gamma = 0$ and fixed rheometer head (θ is constant), "F2" for a frozen granulate and relaxed rheometer head ($T = 0$), and "R" for relaxation experiments at $\Gamma > 0$.

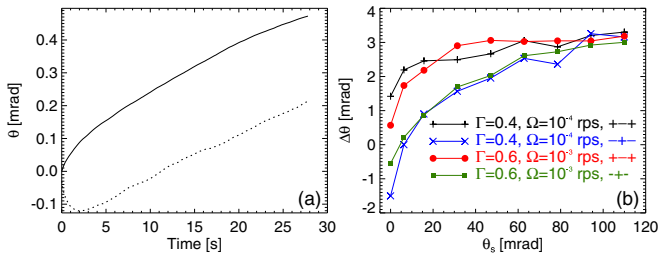

FIG. 2. (Color online) (a) Examples of relaxation curves in stage R. The solid line shows a typical case for $\Gamma = 1$, $\Omega = 0.316 \times 10^{-4}$ rps, and $\theta_s = 100$ mrad. The dashed line reflects a more complex case with a nonmonotonic transient where the preshear was opposite to stage S and where t_s is very short so that the system is not in a simple anisotropic state ($\Gamma = 0.6$, $\Omega = 10^{-3}$ rps, and $\theta_s = 6.28$ mrad).xbrk (b) The dependence of $\Delta\theta$ on the (effective) strain θ_s and the relative directions of preshear and evolution stage as indicated (where the rotation rate in the evolution stage is positive) [26].

the system is not sheared-during the entire preshear stage, the vibrations are at Γ. After this preshear, we prepare anisotropic states by shearing the system at constant Ω, Γ for a given time t_s—we define the total strain during stage S as $\theta_s := 2\pi t_s \times \Omega$. The vibrations tune the rheology [23,24] and, as we will show, allow for controlling the anisotropy as well.

(F) Freeze. To determine the anisotropy of the sheared system, we stop the flow. This part of the protocol is convoluted as care has to be taken to prevent disturbances of the anisotropy. For example, abruptly changing the rheometer's driving conditions from strain-rate controlled mode to stress controlled mode with $T = 0$ perturbs the packing due to inertial effects. Moreover, the flexure that couples disk and rheometer is under tension during stage S, and this tension needs to be relaxed without perturbing the packing.

We therefore adopt a two step protocol. We first (F1) switch from finite Ω to zero, keeping the rheometer in strain-rate control and then immediately afterwards stop the shaking. The system is now frozen: Particles do not move, and the anisotropic fabric is preserved in the packing. We then (F2) switch the rheometer to torque control at $T = 0$ to relax the stresses in the granulate. The flexure then relaxes, leading to damped oscillations of the rheometer's head. We note that during these oscillations the disk remains jammed in the granular medium as the stresses encountered are less than the $\Gamma = 0$ yield stress [23,24]. After the oscillations have died down, stage F is finished, and the net shear stress in the granular medium is zero. However, the anisotropy present in the flowing state is preserved in the granulates fabric. We have checked that the results detailed below are robust with respect to details of the F protocol (e.g., smoothly ramping down Γ instead of a sudden stop or stepping down T in multiple steps).

(R) Probe anisotropy by relaxation. To probe the anisotropy we now impose $\Gamma = \Gamma_{\text{probe}} = 0.4$, keeping $T = 0$. This leads to a rotation of the disk, purely caused by the relaxation of the materials anisotropy. As illustrated in Fig. 1(b), we observe that this relaxation always counters the flow direction in stage I. Hence, a symmetry-breaking field present in the granulate, which we identify as the anisotropy due to flow, drives the counterflow relaxation of the disk in stage R. During relaxation, we probe the angular coordinate of the rheometer $\theta(t)$ at a sample rate of 5 Hz for a total duration of 28 s. We note that since $T = 0$, the flexure remains relaxed and the orientation of the rheometer head and disk remain equal so that $\theta(t)$ accurately describes the rotation of the buried disk. We have checked that other values of Γ_{probe} lead to similar conclusions—the value of 0.4 is chosen at gives relaxation times that can be probed conveniently. We repeat all experiments five times and report averaged measurements, except for $\Omega < 10^{-5}$ rps where we average over three runs.

Phenomenology. We prepare anisotropic states by shearing the system at constant Ω, Γ for a given time t_s after preshear. In Fig. 2(a) we show two examples for the evolution of θ when probed in the relaxation phase, showing significant qualitative differences. For t_s sufficiently large, the relaxation is monotonic (full curve), whereas for small t_s (where in addition the preshear and shear stage have flow in opposite directions) $\theta(t)$ is nonmonotonic (dashed curve). Such complex behavior arises as the anisotropy after the preshear phase in general is different from the steady state anisotropy in the S phase—in particular when the preshear and shear stage have opposite flow directions—which leads to a dependence on t_s.

We now show that for sufficiently large t_s, the anisotropy is well defined. We follow $\theta(t)$ for a range of Ω, Γ, and t_s and for two preshear protocols where the final preshear direction is either the same $(+-+)$ or the opposite $(-+-)$ to the positive shear direction used in the preparation stage S. We characterize such complex curves with $\Delta\theta := \theta(t = 28s)$. In Fig. 2(b) we show $\Delta\theta$ as a function of the effective strain $\theta_s = 2\pi t_s \Omega$ for two different sets of values for Γ and Ω and for both $(+-+)$ and $(-+-)$ preshear protocols. When the preparation stage is short (small t_s), the anisotropy of the packing is essentially given by the preshear, and we observe $\Delta > 0$ for both $(+-+)$ protocols, and $\Delta < 0$ or both $(-+-)$ protocols—as expected. However, for longer shear times t_s, $\Delta\theta$ reaches a plateau for $\theta_s \gtrsim 100$ mrad. Hence, for a sufficiently long shear duration of the shear, the anisotropy becomes independent of the preshear protocol and is a well-defined quantity.

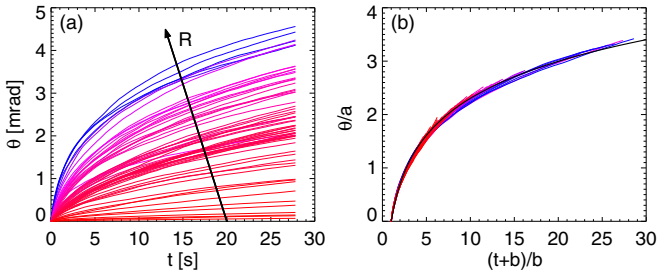

FIG. 3. (Color online) (a) $\theta(t)$ relaxation curves for the full range in Γ and Ω. From bottom (red) to top (blue), the initial relaxation R increases. (b) Plotting the data onto the master curve $[\ln(t+b)/b]$ (plotted in thick black) using Eq. (1) shows a very good data collapse.

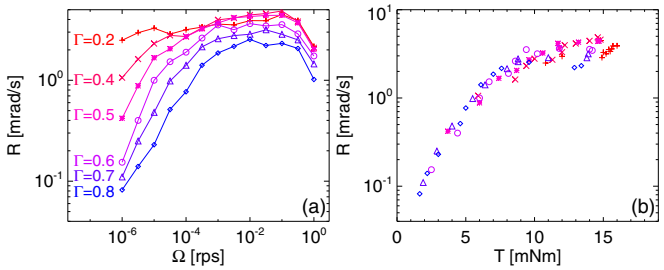

FIG. 4. (Color online) (a) The relaxation R as a function of the control parameters Γ and Ω. (b) The data collapse when we plot R as a function of the steady state driving torque T measured during stage S.

We have also performed experiments (not shown) where, after the preshear, the system is first driven at a fixed vibration intensity Γ_1 and rotation rate Ω_1 for a fixed total rotation angle of the disk θ_1 and then at Γ_2 and Ω_2 for a total disk rotation θ_2. As long as $\theta_2 > 0.1$ rad, the anisotropy only depends on Γ_2 and Ω_2, showing that the steady state anisotropy is not only independent of the preshear orientation, but that in general, the anisotropy goes to a well-defined value.

Logarithmic relaxation. We now probe the steady state anisotropy as a function of the main experimental parameters: the flow rate Ω and the vibration intensity Γ. We vary Γ from 0.2 to 0.8 and have Ω span six decades, from 10^{-6} to 1 rps. We make sure the system is in steady state, which for $\Omega = 10^{-6}$ rps takes approximately 5 h per run.

In Fig. 3(a) we present the relaxation curves $\theta(t)$ for all these experiments where the color represents the relaxation speed at $t = 0$ s. We observe that the magnitude of $\theta(t)$ varies over a large range but that in this case where the system in stage (S) was in steady state, all curves have a similar shape reminiscent of a logarithm. As illustrated in Fig. 3(b), we find that all these data can be fit very well by [27]

$$\theta(t) = a \ln\left(\frac{t+b}{b}\right). \tag{1}$$

As we are interested in the initial rate of change of θ as a proxy for the anisotropy in the frozen state, we define $R := d\theta/dt|_{t=0}$, which using the fit to Eq. (1) can be accurately determined as $R = a/b$. Note that we do not know how R is related to anisotropy in the contact fabric, force fabric, or fraction of sliding contacts—R is an experimentally accessible proxy for the anisotropy.

Collapse of R. In Fig. 4(a) we show the anisotropy R as a function of Ω for vibration amplitudes ranging from $\Gamma = 0.2$ to 0.8. The value of R varies over approximately two decades and shows systematic trends with Ω and Γ. To interpret these qualitatively, consider a competition between flow processes that generate anisotropy and vibrations that relax the anisotropy. In such a picture, the amount of anisotropy in the steady state will diminish for stronger vibrations, precisely as is observed here. Moreover, for slow flows, the relaxation should become more effective, and the anisotropy should go down again as is observed here.

We noted that the variation in R with Γ and Ω is closely related to the variation in the driving torque T as reported in Refs. [23,24]. First, for $\Omega > 0.1$ rps, R decreases—this flow rate corresponds to the transition to inertial flow [13,23,24]. Second, in the quasistatic regime, R and T appear to show the same variations with Ω and Γ. For example, R decreases monotonically with Γ for low Ω, varying over more than a decade—in this same regime, the driving stresses also decrease monotonically with Γ [23,24]. Moreover, for low Γ and $10^{-4} < \Omega < 10^{-1}$, R is essentially independent of Ω—precisely in this range, the flow is essentially rate independent [23].

In Fig. 4(b) we plot R as a function of T (as measured in stage S), restricting ourselves to data for which $\Omega \leqslant 0.1$ rps. We observe a surprisingly good data collapse, in particular for small T, without any adjustable parameters. This shows that in the absence of inertial effects, anisotropy and resistance to flow are strongly related. Intriguingly, our data show that R becomes very small when T becomes small. This suggests that the buildup of anisotropy is crucial for granular media to resist flow and that in the absence of anisotropy, this resistance would be minute—consistent with the observation of a large stress drop during flow reversal experiments [2,7]. Our experiments thus evidence a deep connection between anisotropy and granular rheology.

Discussion and outlook. We have introduced an experimental protocol to probe the anisotropy of granular media by probing the relaxation of frozen packings under weak vibrations. Our data provide strong evidence that resistance to flow and anisotropy go hand in hand. Moreover, our data suggest that in the absence of anisotropy, the resistance to flow is minute [2].

Of course, our experiments are indirect, and more validation of our technique is warranted. Nevertheless, we believe our data provide strong evidence that the relaxation under vibrations is due to and probes the anisotropy. One crucial piece of information is that the direction of relaxation is always opposite to the preceding flow, showing that symmetry breaking due to flow must be crucial. Moreover, the observed increase and decrease in R with Ω and Γ is consistent with a simple picture of flow generating and vibration relaxing anisotropy. One may wonder about the role of packing density. We note that the qualitative trends in R are inconsistent with a purely density based picture. Vibrations tend to compactify granular media, and denser media resist flow more strongly, opposite to what we find here. Hence, a picture in which the

variations in anisotropy are dominant, instead of changes in packing density, appears to be correct.

Flow induced anisotropy of the granular fabric is readily observed in numerical simulations [20], and it will be interesting to see if such simulations are able to capture the observed effect of vibrations on anisotropy and the rheology of granular flows. We note that the idea of a backstress, generated in sheared granular materials, is reminiscent of kinematic hardening models [28] and suggest that such ideas may be a fruitful starting point for more refined constitutive relations and models of nonstationary granular flows [4,13]. Finally, we suggest that anisotropy dominated effects are not only limited to granular media, but also may be observable in other athermal, particulate media, such as colloidal and macrosuspensions, foams, and emulsions.

Acknowledgments. We acknowledge discussions with J. Dijksman and O. Dauchot and technical support from J. Mesman. G.H.W. acknowledges funding by FOM.

[1] O. Reynolds, Philos. Mag. **20**, 469 (1885).
[2] M. Toiya, J. Stambaugh, and W. Losert, Phys. Rev. Lett. **93**, 088001 (2004).
[3] R. M. Nedderman, *Statics and Kinematics of Granular Materials* (Cambridge University Press, Cambridge, UK, 1992).
[4] K. Kamrin and G. Koval, Phys. Rev. Lett. **108**, 178301 (2012).
[5] D. L. Henann and K. Kamrin, Phys. Rev. Lett. **113**, 178001 (2014).
[6] D. Henann and K. Kamrin, Proc. Natl. Acad. Sci. USA **110**, 6730 (2013).
[7] B. Utter and R. Behringer, Eur. Phys. J. E: Soft Matter Biol. Phys. **14**, 373 (2004).
[8] T. Majmudar and R. Behringer, Nature (London) **435**, 1079 (2005).
[9] E. Wandersman and M. van Hecke, Europhys. Lett. **105**, 24002 (2014).
[10] N. Guo and J. Zhao, Comput. Geotech. **47**, 1 (2013).
[11] M. Oda, S. Nemat-Nasser, and J. Konishi, Soils Found. **25**, 85 (1985).
[12] E. Collins and B. Muhunthan, Geotechnique **53**, 611 (2003).
[13] P. Jop, J. Forterre, and O. Pouliquen, Nature (London) **441**, 727 (2006).
[14] GDR MiDi, Eur. Phys. J. E: Soft Matter Biol. Phys. **14**, 341 (2004).
[15] O. Pouliquen and Y. Forterre, J. Fluid Mech. **453**, 133 (2002).
[16] K. A. Reddy, Y. Forterre, and O. Pouliquen, Phys. Rev. Lett. **106**, 108301 (2011).
[17] K. Nichol, A. Zanin, R. Bastien, E. Wandersman, and M. van Hecke, Phys. Rev. Lett. **104**, 078302 (2010).
[18] K. Nichol and M. van Hecke, Phys. Rev. E **85**, 061309 (2012).
[19] We note that classical approaches, such as critical-state theory, are not able to correctly reproduce the flow profiles of slow granular flows, such as those for the split-bottom shear cell. It is even less clear how critical-state theory would deal with the vibrated or agitated systems that we deal with here.
[20] N. Kumar, S. Luding, and V. Magnanimo, Acta Mechanica **225**, 2319 (2014); O. I. Imole, M. Wojtkowski, V. Magnanimo, and S. Luding, Phys. Rev. E **89**, 042210 (2014); A. Singh, V. Magnanimo, K. Saitoh, and S. Luding, New J. Phys. **17**, 043028 (2015).
[21] J. H. Snoeijer, W. G. Ellenbroek, T. J. H. Vlugt, and M. van Hecke, Phys. Rev. Lett **96**, 098001 (2006).
[22] D. Howell, R. P. Behringen, and C. Veje, Phys. Rev. Lett. **82**, 5241 (1999).
[23] J. A. Dijksman, G. H. Wortel, L. T. H. van Dellen, O. Dauchot, and M. van Hecke, Phys. Rev. Lett. **107**, 108303 (2011).
[24] G. H. Wortel, J. A. Dijksman, and M. van Hecke, Phys. Rev. E **89**, 012202 (2014).
[25] J. Dijksman and M. van Hecke, Soft Matter **6**, 2901 (2010).
[26] The counterclockwise or clockwise relaxation of the probe depends on the direction of the flow preceding the relaxation experiments. From now on, we define the sign of θ such that it is positive.
[27] The data must deviate from this fit at large t, but this is irrelevant for the determination of R.
[28] A. Gajo and D. M. Wood, Int. J. Numer. Anal. Methods Geomech. **23**, 925 (1999).